Quasi-Steady Plasma Acceleration

KENN E. CLARK* AND ROBERT G. JAHN†
Princeton University, Princeton, N. J.

A coaxial plasma accelerator driven by protracted pulses of current in the range of 10^4–10^5 amp and synchronized mass flows from 1.0 to 50 g/sec of argon attains, after some tens of μsec, a stable acceleration mode which replicates in every observable detail steady flow self-field magnetoplasmadynamic acceleration. This "quasi-steady" discharge form is characterized by constant terminal voltage and arc current, a diffuse, fixed current distribution within the discharge, and a steady plasma efflux at velocities in excess of 10^4 m/sec. The device is thus of interest as a simulator of self-field arcjet operation which is much more amenable to detailed diagnostic study, and which can be extended to multimegawatt power levels totally inaccessible to steady flow testing. In addition, it may presage a repetitively pulsed quasi-steady thruster of high-efficiency and variable thrust capability.

I. Introduction

STABILIZATION of the discharge current patterns of pulsed plasma accelerators into steady diffuse phases for pulse lengths above a few microseconds has been demonstrated for several electrode geometries.[1–4] Study of this "quasi-steady" phase for an electrode configuration resembling the steady state magnetoplasmadynamic (MPD) arcjet[5–7] is attractive from several points of view. First, such quasi-steady operation permits application of transient diagnostic techniques within the arc chamber and exhaust plume, environments normally too hostile for detailed study in steady flow operation, even at the 100 kw minimum power level required for self-field acceleration. Second, the quasi-steady experiment permits extension of MPD operation to multimegawatt power levels totally inaccessible to steady experiments because of heat transfer, power supply, and gas handling limitations. Such high-power operation is of basic interest because the over-all efficiency of the MPD arc has been observed to improve as the power level is increased, and may also be instructive for advanced mission studies. For example, certain projections of manned missions to the near planets favor propulsion system power in the range of 1–10 Mw[8,9]; quasi-steady MPD studies may provide an initial hint on the feasibility of single thruster operation in this range. Finally, the quasi-steady acceleration mode may prove to be an interesting propulsion technique in its own right. In particular, it is possible that intermittent long-pulse operation may combine the benefits of high-power MPD operation with tolerable average power consumption and simple variable thrust capability via duty cycle adjustment.

II. Experimental Design

Proper quasi-steady operation requires rather precise correlation of the injected mass pulse with the applied current pulse. With reference to Fig. 1, the injected mass flow rate, $\dot{m}$, must rise quickly (τ_R) to a steady value, and remain at that value until after the current pulse J has been completed (τ_M). The current pulse cannot be initiated until the chamber pressure has reached a steady value corresponding to the injected mass flow rate (τ_A), but this time must be sufficiently short that the vacuum tank back pressure is not compromised by the predischarge flow. After the appropriate delay (τ_D) the current pulse should rise quickly (τ_r) to some steady value, and last for a time characteristic of the current source (τ_L). Before the arc discharge can be considered to be operating as a true quasi-steady accelerator, the chamber pressure p_c must readjust to its "hot" operating condition (τ_F), the exhaust plume must reach some stabilized current density pattern (τ_s), and the cathode must attain steady thermionic emission (τ_c). If these several time constants are of commensurate magnitudes and the various events are properly synchronized, there remains an interval (τ_Q) during which reasonable simulation of steady operation should prevail.

In the experiment described here, the driving current pulse is provided by a bank of 40 × 3.2 μfarad capacitors arranged in an LC ladder network.[10] Varying the interstation inductance yields a variable amplitude, variable length pulse covering the range from 140 ka × 20 μsec to 4.4 ka × 600 μsec. A separate gas-triggered, closed-chamber discharge switch[11] transfers the 10-kv bank voltage to the electrode assembly.

A shock tube is used to provide the tailored mass injection pulse. As seen in Fig. 2, this tube is mounted directly behind

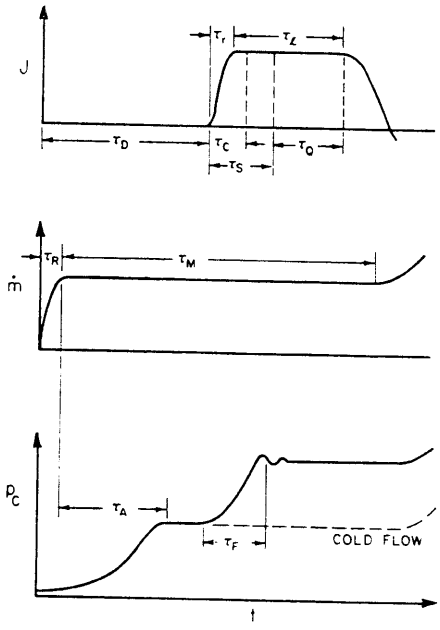

Fig. 1 Characteristic times for current and mass flow pulses.

Presented as Paper 69-267 at the AIAA 7th Electric Propulsion Conference, Williamsburg, Va., March 3–5, 1969; submitted March 18, 1969, revision received July 28, 1969. This program is supported by NASA Grant NGL 31-001-005.

* Research Staff Member, AMS Department, Guggenheim Aerospace Propulsion Laboratories. Member AIAA.

† Professor of Aerospace Sciences, AMS Department, Guggenheim Aerospace Propulsion Laboratories. Associate Fellow AIAA.

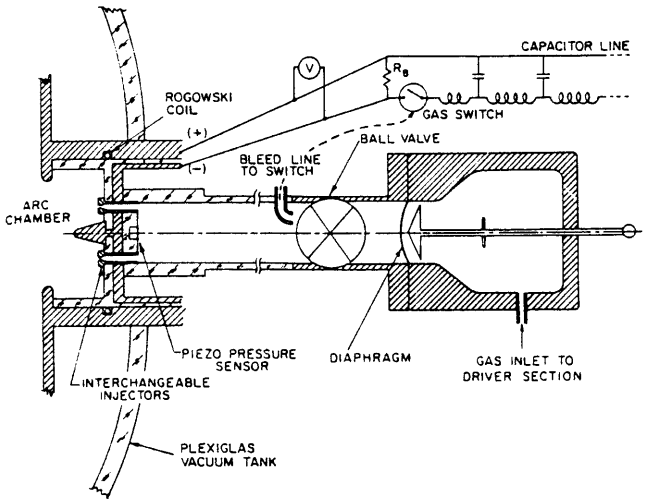

Fig. 2 Schematic of accelerator electrical and mass injection systems.

the arc chamber with six interchangeable injection tubes connecting the end of the Plexiglas driven section to the discharge chamber. The tube is not operated in the conventional manner in the sense that the driven section is not maintained at a continuum pressure level, but is pumped out to the back pressure of the vacuum tank, less than 10^{-5} torr. The driver section is normally pressurized to 35 psia. Upon rupturing the diaphragm, the pressure history at the driven section end wall, and thus the mass injection history, is formed by the superposition of the initial diffuse compression, the rear portion of the initial rarefaction wave which is convected downstream, and the reflection of the rarefaction head off the driver end wall. The tube length is therefore kept relatively short to reduce the time to attain steady end wall pressure. The particular configuration shown, consisting of a driven section 30 in. long × $2\frac{3}{8}$ in. i.d., and driver section 6 in. long × $4\frac{3}{4}$ in. i.d., is capable of providing mass flow rates up to 50 g/sec for 3 msec, with a rise time of about 1 msec.

A piezoelectric pressure sensor is mounted in the driven section end wall to monitor end wall pressure time history and to provide a time mark for synchronizing the mass and current pulses. The gas-triggered switch is supplied by a bleeder tube from the upstream portion of the shock tube channel. Adjusting the length and size of this line controls the discharge delay time (τ_D). Figure 3 shows a typical trace of the end wall pressure history p_w compared with the arc current. In this particular case, the mass flow rate reaches a level of about 36 g/sec after 1 msec. The discharge is triggered at roughly 1.3 msec, a time verified to be sufficiently long to allow the chamber pressure to reach an equilibrium value. Although the capacitor line rings down in a fashion characteristic of its mismatch to the load, only the first half cycle is normally employed in this experiment.

Proper simulation of steady MPD operation also involves replication of the essential features of the arc chamber geometry. Based on the typical configuration of a central,

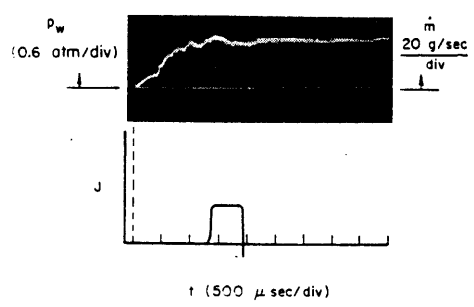

Fig. 3 Current pulse synchronization with injected mass.

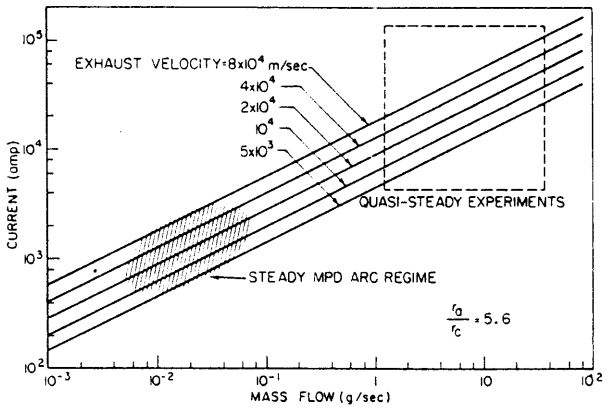

Fig. 4 Relation of current, mass flow, and exhaust velocity for a coaxial plasma accelerator.

conically tipped cathode, a pierced anode slightly downstream and coaxial with it, and axial gas injection upstream of the electrode gap, there remains only the choice of absolute dimensions on the basis of some appropriate scaling criterion. For this purpose, one might require duplication of the thrust density, which for a given exhaust velocity implies equal power density and mass flux density, or, alternatively, a magnetic interaction parameter might be invoked. Actually, these two approaches yield essentially the same conclusion, by virtue of the relation between the arc current and the total electromagnetic thrust[12]:

$$T = (\mu J^2/4\pi)[\ln(r_a/r_c) + \tfrac{3}{4}] = \dot{m}u \qquad (1)$$

where T = thrust, J = total current, r_a, r_c = effective radii of discharge attachment on anode and cathode, $\dot{m}$ = mass flow rate, u = exhaust velocity. That is, for a given exhaust velocity, the thrust density, mass flux density, and power density all scale as $(J^2/A)\ln(r_a/r_c)$. Presuming the insensitive logarithmic factor to be approximately matched by retaining the same ratio of anode orifice to cathode diameters, the absolute values of these radii should thus be scaled linearly with the discharge current. Since we choose to cover the current range from 4000 to 140,000 amp, compared to the 2000 to 4000 amp range of steady devices, their typical anode orifice radius of $\frac{1}{4}$ in. should here be increased by about one order of magnitude. The selected value of 2 in. actually permits study of substantially higher ranges of thrust density than attainable in the steady accelerators.

The thrust relation (1) is plotted in Fig. 4 in a slightly different form to display the corresponding mass flow rates required to achieve an interesting range of exhaust velocities for these large currents. For the chosen anode radius, these transcribe into mass flux densities from 0.10 to 4.30 kg/m² sec, a range which overlaps and extends the steady flow range of 0.15 to 2.00 kg/m² sec.[13,14]

The outer face of the anode is allowed to extend almost to the vacuum tank wall, a radius of 17 in., in order to minimize the anode fall voltage[15] and to allow full development of the exhaust plume. The 2% thoriated tungsten cathode has a $\frac{3}{4}$-in.-diam base and extends 1 in. into the arc chamber. A photograph of the chamber showing the cathode, injector plugs, and part of the anode is shown in Fig. 5.

The assembled chamber and mass injection system are installed in a 3-ft-diam × 6-ft-long Plexiglas vacuum tank described elsewhere.[16] Before each shot the tank is evacuated

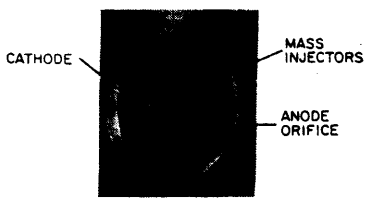

Fig. 5 View of accelerator chamber.

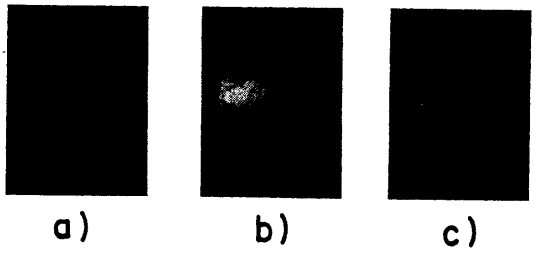

Fig. 6 Stabilized exhaust luminosity patterns for various mass flow rates at 17.5 ka: a) $\dot{m}$ = 1.2 g/sec, b) $\dot{m}$ = 5.9 g/sec, c) $\dot{m}$ = 36.0 g/sec.

to less than 10^{-5} torr, at which pressure the mean free path of the resident particles is considerably larger than the tank dimension.

The operation sequence of the system begins with pressurization of the shock tube driver to 35 psia, and charging of the capacitor line to 10 kv. The diaphragm is then ruptured with a springloaded blade. The pressure wave propagating down the tube is first sampled by the small bleed tube that begins filling of the gas-triggered switch, and then is recorded by the end wall piezocrystal. This signal triggers an oscilloscope to display the delay time until discharge initiation on a record of the integrated response of a Rogowski coil enclosing the chamber as shown in Fig. 2. The Rogowski coil also triggers a second oscilloscope that sweeps at a much faster rate and monitors other diagnostic measurements, such as the electrode voltage, magnetic probe signatures, etc., during the first half cycle. To prevent spurious electromagnetic noise from distorting these traces, the oscilloscopes are enclosed in a screen room which is grounded to the anode by a 3-ft-wide by 15-ft-long copper ground plane. All leads from the Rogowski coil, voltage probe, and piezocrystal are dressed closely to this ground plane.

III. Luminosity Patterns

Sample photographs of quasi-steady discharges in argon are shown in Fig. 6. These photographs, taken through a 5 μsec Kerr-cell shutter, display luminosity patterns for three different mass flow rates, $\dot{m}$ = 1.2, 5.9, and 36.0 g/sec, at a common current level of 17.5 ka. With reference to Fig. 4, these mass flows define nominal exhaust velocities of 6.3×10^4, 1.2×10^4, and 2.1×10^3 m/sec, respectively. Just as in these photographs, over the entire range of test conditions indicated in Fig. 4, the discharge is invariable axisymmetric with no evidence of spoking. Note also the sharp demarcation between dark and light at the upstream edge of the luminous patterns, particularly in the tightly confined portion near the cathode tip. The effect is most pronounced for the low mass flow rate, and is not readily correlated with any features of the current density patterns discussed later. In general, it is found that the characteristics of such photographs are typical of the nominal exhaust velocity, i.e., it is the combination of current and mass flow rate which influences the discharge appearance rather than either separately.

IV. Terminal Voltage

The measurement of total voltage across the discharge chamber is instructive for several reasons: first, the effectiveness of the electromagnetic acceleration process should be reflected in a $\mathbf{u} \times \mathbf{B}$ or back EMF component. Second, little is known about the resistive component of discharge voltage at current levels above 10^4 amp. In the past, voltage measurements have been used extensively in steady state experimentation to compare arc performance with theoretical acceleration models. Figure 7 displays a typical voltage-current trace for the 17.5 ka pulse and an argon mass flow rate of 3.8 g/sec. The slight droop in the current is due to the time constant of the integrating circuit; larger time constants yield perfectly flat profiles, but have less sensitivity. The sharp drop in the voltage signal at the beginning of the pulse from the applied 10 kv to about 180 v is interpreted as signifying the attainment of thermionic emission by the cathode, since any other mechanism would require substantially higher voltages to support this current density.

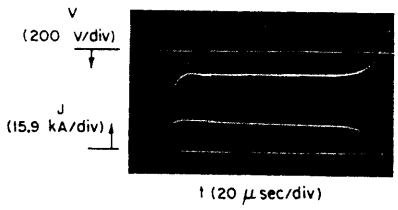

Fig. 7 Typical accelerator voltage-current history: J = 17.5 ka, $\dot{m}$ = 3.8 g/sec.

Steady voltage traces of this sort are observed over the entire range of current and mass flow operation. As summarized in Fig. 8, these raw voltage data show the general trends of decrease with mass flow, and increase with discharge current anticipated from the electromagnetic thrust model. Precise correlation with any analytical model is difficult because of inadequate knowledge of the various power loss mechanisms acting in the discharge. Specifically, the measured voltage must reflect not only the electromagnetic acceleration process, but also the energy transfer to the electrode surfaces via their respective falls, and the electrothermal energy deposition into the gas stream via joule heating in the body of the discharge, i.e.,

$$V = V_b + V_a + V_c + V_t \tag{2}$$

where $V_i = \dfrac{\text{electromagnetic thrust power}}{\text{discharge current}} =$

$$\frac{T^2}{2\dot{m}J} = \frac{\mu^2 J^3}{32\pi^2 \dot{m}} \left[\ln\left(\frac{r_a}{r_c}\right) + \frac{3}{4} \right]^2 \tag{3}$$

$$V_a = \frac{\text{power to anode}}{\text{discharge-current}} \tag{4}$$

$$V_c = \frac{\text{power to cathode}}{\text{discharge current}} \tag{5}$$

$$V_t = \frac{\text{electrothermal power to gas}}{\text{discharge current}} \tag{6}$$

The magnitudes of V_a, V_c, and V_t, and their dependence on $\dot{m}$ and J are poorly known. It seems reasonable that V_c should be slightly higher than the work function of tungsten,

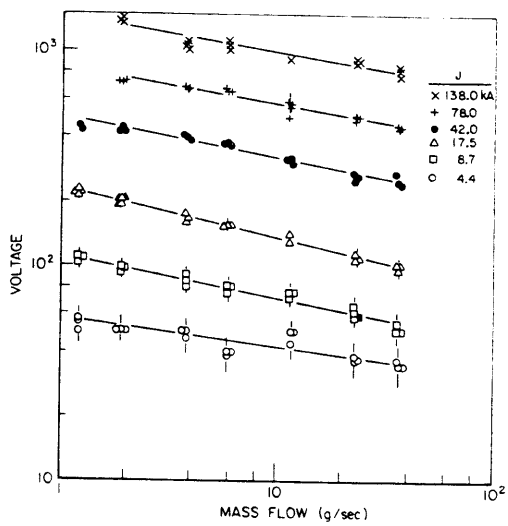

Fig. 8 Summarized voltage variation with current and mass flow rate.

say ~5 v, a value consistent with certain unpublished electric probe studies of similar discharges in this laboratory. These same studies indicate anode falls in the vicinity of 15 v up to currents of 300 ka. The dependence of V_a and V_c on $\dot{m}$ and J, although not carefully studied, appears to be weak.

The electrothermal power input encompasses the ionization of the flow, and all internal excitation, random thermal, and radiation processes which attend it, as well as the joule dissipation associated with passage of the discharge current through the ionized medium. Some of this input may be recovered as useful thrust by electrothermal conversion in the exhaust plume and the remainder constitutes a frozen flow loss: the distinction is immaterial so far as the contribution to the terminal voltage is concerned. It is common practice in estimating the electrothermal voltage to assume that the ionization potential effectively limits the temperature of the particulate species in the plasma, and even to make the approximation that the sole significant energy sink is the single ionization of each incoming particle:

$$V_t \approx (\dot{m}/M)e\mathcal{E}_I/J \tag{7}$$

where M is the atomic mass, e the electronic charge, and $\mathcal{E}_I$ the first ionization potential. A second approximation to this approach inserts a constant factor to cover the excitation, radiation, and random thermal modes that accompany this ionization level. The significant element in either formulation is the linear coupling of V_t to the mass flow, and this feature is clearly denied by our total voltage data. Figure 9 shows the experimental data for $J = 17.5$ ka compared to calculated values of V_b, corrected by $V_a + V_c = 20$ v. The difference curve, which must be V_t, rather than increasing linearly with $\dot{m}$, reaches a constant asymptote, $\hat{V}_t$, implying no further thermal input regardless of the increase in mass flux. Similar behavior is found at other current levels, with $\hat{V}_t$ increasing linearly with current at a slope of about 4 v/ka, i.e., in this domain the plasma acts as an ohmic medium, with a fixed resistance of 0.004 ohm.

V. Current Density Distribution

Enclosed current contours in the exhaust plume and discharge chamber are mapped with standard magnetic probes of #38 Formvar wire, oriented in the r,z plane. Their integrated signatures present local time histories of the azimuthal magnetic field; cross plotting then yields the spatial distribution of the field at any given time, which, for the observed azimuthal symmetry, is directly proportional to the fraction of the discharge current enclosed by a circle at the given radius. In operation, four probes, mounted on a movable carriage within the exhaust tank, are positioned remotely between each of a sequence of discharges to accumulate the

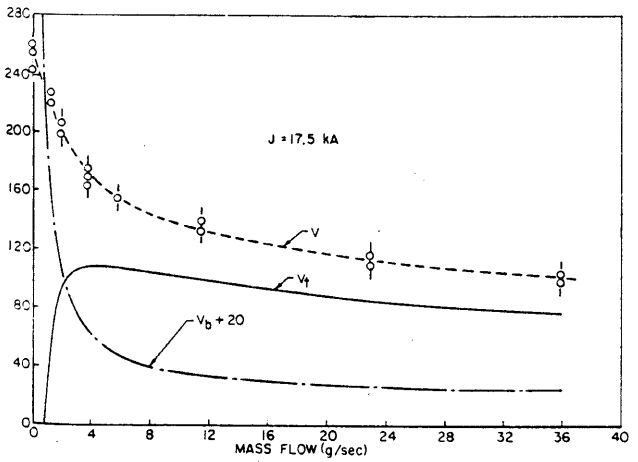

Fig. 9 Voltage component variation with mass flow rate at 17.5 ka.

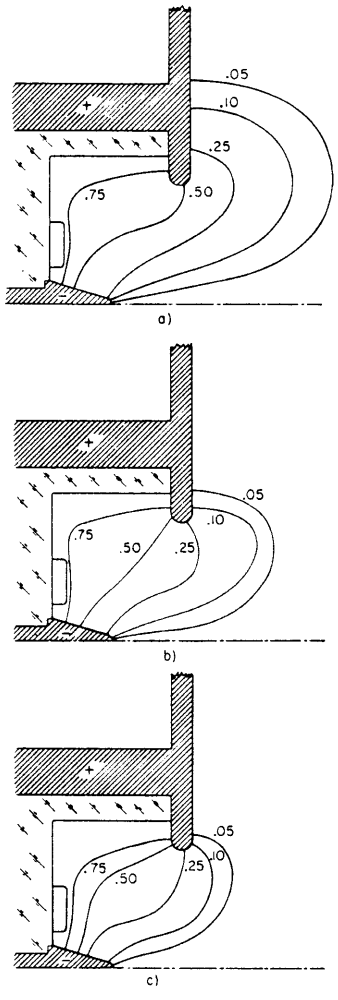

Fig. 10 Fractional contours of enclosed current in accelerator chamber and exhaust at 17.5 ka: a) $\dot{m}$ = 1.2 g/sec, b) $\dot{m}$ = 5.9 g/sec, c) $\dot{m}$ = 36.0 g/sec.

necessary matrix of data. Figure 10 displays typical maps of enclosed current contours in the chamber and near-exhaust for quasi-steady conditions of 1.2, 5.9, and 36.0 g/sec mass flow at a current level of 17.5 ka. As in the luminosity photographs, these figures exhibit characteristics common to the particular nominal exhaust velocity, regardless of the individual level of current or mass flow. First, for the higher velocities, Fig. 10a, the given contours are slightly extended downstream into the plume; for the lower velocities, Fig. 10c, the contours are withdrawn slightly upstream into the chamber. Second, for all quasi-steady conditions observed, no significant amount of current extends farther than one orifice diameter outside of the chamber, either axially or radially. Third, the bulk of the current does not coincide with the luminosity patterns, such as those shown in Fig. 6. This is in contrast to most pulsed plasma accelerators where the luminosity provides a very good indication of the maximum current density location. Fourth, in all gases studied, the current attachment on the cathode completely covers the surface, i.e., the effective radius of attachment for purposes of relation (1) is the maximum material radius. As the nominal exhaust velocity increases, the distribution shifts from a fairly uniform one to one more peaked toward the cathode tip.

VI. Velocity Measurements

To this point, the observed performance of the accelerator has been catalogued in terms of the nominal velocity called out by relation (1) or Fig. 4 for given inputs of mass flow and current. This relation is based on many assumptions of flow and field geometry, of lack of significant electrothermal conversion, and in particular of complete utilization of the injected working fluid, whose validity are not readily assessed experimentally. The last assumption is particularly critical

to the exhaust velocity actually attainable in the accelerator, since any failure of the discharge to accelerate all of the injected flow, or any acquisition of spurious mass from electrodes, insulator, or background gas, distorts the $\dot{m}$ factor in Eq. (1). For these reasons, experimental determination of the actual velocity field of the exhaust plume is highly desirable. Unfortunately, this measurement, both in steady flow devices and in this quasi-steady version, has proven difficult. Tedious Doppler shift techniques have provided a few isolated data points for the former,[17,18] but are less applicable here. Exploratory experiments with displaced pairs of biased double electrostatic probes indicate quasi-steady velocities on the accelerator axis of approximately 2.5×10^4 m/sec for the $J = 17.5$ ka, $\dot{m} = 5.9$ g/sec combination. A gridded ion energy analyzer returns a similar value for the same conditions. Description of these techniques and more complete presentation of their results appears in another reference.[19] Considering the uncertainties in these measurements, and our lack of knowledge of the remainder of the flow field, they compare reasonably with the nominal value of 1.2×10^4 m/sec derived from relation (1), and suggest that in this respect the electromagnetic model has some relevance to the experimental situation.

VII. Summary

By appropriate sequencing of tailored current and mass pulses, a quasi-steady acceleration phase has been achieved in a coaxial geometry resembling the steady, self-field MPD arcjet. Detailed measurements have shown that all pertinent arc processes become steady on a time scale short compared to the current pulse length and that a high-velocity plasma is thereafter continuously ejected from the accelerator. Terminal voltage measurements, Kerr-cell photography, and time resolved magnetic field distributions are readily attained, and illuminate certain of the arc acceleration characteristics. In particular, the voltage measurements show a current and mass flow dependence which is not in agreement with estimates based on the ideally anticipated voltage components. Magnetic field measurements show that the stabilized current zone completely fills the arc chamber and covers the exposed cathode surface with a nearly uniform current density. Yet, little of this distribution spreads outside the anode orifice and virtually none extends beyond one orifice diameter either radially or axially. Preliminary velocity measurements confirm operation in a range of exhaust speeds of interest to advanced propulsion.

References

[1] Eckbreth, A. C., Clark, K. E., and Jahn, R. G., "Current Pattern Stabilization in Pulsed Plasma Accelerators," *AIAA Journal*, Vol. 6, No. 11, Nov. 1968, pp. 2125–2132.

[2] Eckbreth, A. C., "Current Pattern and Gas Flow Stabilization in Pulsed Plasma Accelerators," Ph.D. thesis, Dec. 1968, Princeton Univ., Princeton, N. J.

[3] Burton, R. L. and Chang, O. V., "Acceleration Process in a Stabilized High-current Arc," *AIAA Journal*, Vol. 6, No. 11, Nov. 1968, pp. 2190–2192.

[4] Gooding, T. J., private communication, 1967, General Dynamics Corp., San Diego, Calif.

[5] Nerheim, N. M. and Kelly, A. J., "A Critical Review of the State-of-the-art of the MPD Thrustor," *AIAA* Paper 67-688, Colorado Springs, Colo., 1967.

[6] Clark, K. E. and Jahn, R. G., "The Magnetoplasmadynamic Arcjet," *Astronautica Acta*, Vol. 13, No. 4, July-Aug. 1967, pp. 315–325.

[7] Noeske, H. O., "The Coaxial MPD Engine, A State-of-the-art Review," *AIAA* Paper 66-242, San Diego, Calif., 1966.

[8] "Low Acceleration Space Transportation System Study," Final Report, Volume II: Technical Report, GE-ANSO Document 6300-260-2, Philadelphia, Pa., Oct. 1967, General Electric.

[9] Masey, A. C., Dugan, D. W., and Pitts, S. W., "Application of Combined Electric, High-thrust Propulsion Systems," *Journal of Spacecraft and Rockets*, Vol. 5, No. 7, July 1968, pp. 785–791.

[10] Black, N. A., "Dynamics of a Pinch Discharge Driven by a High-Current Pulse-forming Network," Ph.D. thesis, April 1966, Princeton Univ., Princeton, N. J.

[11] Jahn, R. G., von Jaskowsky, W., and Casini, A. L., "Gas-triggered Pinch Discharge Switch," *The Review of Scientific Instruments*, Vol. 36, No. 1, Jan. 1965, pp. 101–102.

[12] Jahn, R. G., *Physics of Electric Propulsion*, McGraw-Hill, New York, 1968, Chap. 8.

[13] Malliaris, A. C., "Plasma Acceleration in an Electrical Discharge by the Self-induced Magnetic Field," *Journal of Applied Physics*, Vol. 38, No. 9, Aug. 1967, pp. 3611–3619.

[14] Hügel, H., "Self-magnetic Effect in Arcjet Engines," *AIAA Journal*, Vol. 6, No. 8, Aug. 1968, pp. 1573–1575.

[15] "Pulsed Electromagnetic Gas Acceleration," Rept. 634k, Dept. of Aerospace and Mechanical Sciences, July 1968, Princeton Univ., Princeton, N. J.

[16] Jahn, R. G. and Clark, K. E., "A Large Dielectric Vacuum Facility," *AIAA Journal*, Vol. 4, No. 6, June 1966, p. 1135.

[17] Malliaris, A. C. and Libbey, D. R., "Velocities of Neutral and Ionic Species in an MPD Flow," *AIAA* Paper 69-109, New York, 1969.

[18] Kogelschatz, U., "Doppler Shift Measurements of Axial and Rotational Velocities in an MPD Arc," AIAA Paper 69-110, New York, 1969.

[19] Jahn, R. G. et al., "Acceleration Patterns in Quasi-Steady MPD Arcs," AIAA Paper 70-165, New York, 1970.